scription.
[14]G. C. Nelson, B. G. Saunders, and S. I. Salem, At. Data 1, 377 (1970).
[15]S. I. Salem, in *Inner Shell Ionization Phenomena and Future Applications*, edited by R. W. Fink, S. T. Manson, J. M. Palms, and P. V. Rao (North-Holland, Amsterdam, 1972), p. 285.
[16]W. H. McMaster, N. Kerr Del Grande, J. H. Mallet, and J. H. Hubbell, Lawrence Radiation Laboratory Report No. UCRL-50174, 1969, Sec. II, Rev. I (unpublished).
[17]R. W. James, *The Optical Principles of Diffraction of X-rays* (Cornell U.P., Ithaca, N. Y., 1965).
[18]*International Tables for X-Ray Crystallography* (Kynock, Birmingham, England, 1968), Vol. III.
[19]S. I. Salem, R. T. Tsutsui, and B. A. Rabbani, Phys. Rev. A 4, 1728 (1971).

PHYSICAL REVIEW A VOLUME 6, NUMBER 6 DECEMBER 1972

Many-Body Calculation of the Photodetachment Cross Section of O^- †

Robert L. Chase* and Hugh P. Kelly
Department of Physics, University of Virginia, Charlottesville, Virginia 22901
(Received 5 July 1972)

Many-body perturbation theory is used to calculate the total photodetachment cross section of O^- from threshold to 1.1 keV. This nonrelativistic calculation uses the velocity form of the dipole approximation. We include the effects of resonances owing to $2s \rightarrow 2p$ and $1s \rightarrow 2p$ excitations. Comparison is made with experiment and other theoretical treatments.

I. INTRODUCTION

The photodetachment cross section of O^- has been the subject of several theoretical and experimental studies, primarily because of its astrophysical applications. The first calculation was performed by Bates and Massey.[1] Since the accurate determination of the electron affinity of oxygen[2] and the accurate measurement of the absolute cross section by Smith,[3] good results in the range from threshold to about 3.2 eV were obtained by improving the Hartree–Fock calculation through the use of polarization potentials.[4–6] Utilizing Temkin's method of polarized orbitals,[7] the calculation of Henry[8] showed good agreement with experiment up to about 3.6 eV.

In order to take into account the effect of electron correlations on the photodetachment cross section of O^-, we present here a detailed calculation of that cross section using the many-body perturbation theory of Brueckner[9] and Goldstone[10] and our techniques for the application of this theory to atoms.[11–14] Recently, the Brueckner–Goldstone theory was used to calculate the photoionization cross section of Fe, both initial- and final-state correlations being included.[15,16]

In Sec. II we discuss the theory. Section III contains the details of the calculation and also the numerical results. We present results for the total photodetachment cross section, contributions to the cross section from the individual subshells, and also our lowest-order results, which are essentially Hartree–Fock results. The discussion and conclusions are presented in Sec. IV.

II. THEORY

In applying many-body perturbation theory to the photoionization problem, we use the perturbation expansion for the frequency-dependent polarizability[14] $\alpha(\omega)$ together with the relation[17]

$$\sigma(\omega) = (4\pi\omega/c)\,\mathrm{Im}\,\alpha(\omega). \tag{1}$$

Here $\sigma(\omega)$ is the photoionization cross section, ω is the photon energy, and c is the speed of light (137.037 in atomic units).

The lowest-order contribution to $\alpha(\omega)$ due to the electronic state $|p\rangle$ is given by[14]

$$-\sum_k |\langle k|z|p\rangle|^2 \left(\frac{1}{\epsilon_p - \epsilon_k + \omega} + \frac{1}{\epsilon_p - \epsilon_k - \omega}\right), \tag{2}$$

where z represents $\sum_{i=1}^N z_i$. Since $\epsilon_p - \epsilon_k + \omega$ may vanish, we add a small imaginary part $i\eta$. We then obtain

$$\lim_{\eta\to 0}(\epsilon_p - \epsilon_k + \omega + i\eta)^{-1} = P(\epsilon_p - \epsilon_k + \omega)^{-1} - i\pi\delta(\epsilon_p - \epsilon_k + \omega), \tag{3}$$

where P represents principal-value integration. Since our continuum states are normalized according to

$$P_{kl}(r) \rightarrow \cos[kr + \delta_l + (q/k)\ln 2kr - \tfrac{1}{2}(l+1)\pi], \tag{4}$$

where $V(r) \rightarrow q/r$ as $r \rightarrow \infty$, we may replace the summation over k in Eq. (2) by $(2/\pi)\int dk$.[11,12] Using Eq. (3) we obtain

$$\mathrm{Im}\,\alpha(\omega) = (2/k_0)\,|\langle k_0|z|p\rangle|^2, \tag{5}$$

where

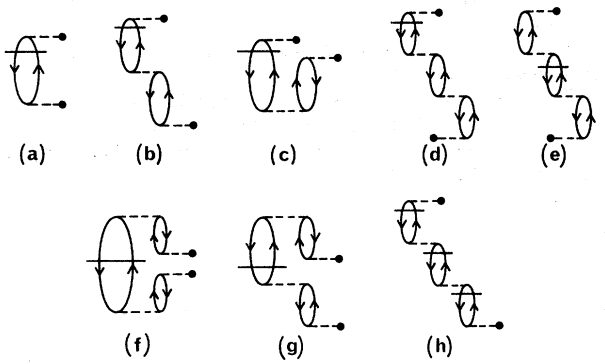

FIG. 1. Diagrams which contribute to the photodetachment cross section or to $\mathrm{Im}\alpha(\omega)$. The horizontal line indicates the denominator contribution is $-i\pi\delta$. The heavy dot indicates the velocity form of the dipole matrix element.

$$k_0 = 2(\epsilon_p + 2\omega)^{1/2}, \tag{6}$$

since for continuum states $\epsilon_k = \frac{1}{2}k^2$.

Substituting Eqs. (2) and (5) into Eq. (1), the lowest-order contribution to $\sigma(\omega)$ is

$$\sigma(\omega) = (8\pi\omega/ck_0)\,|\langle k_0|z|p\rangle|^2 . \tag{7}$$

Further details are given in Refs. 14 and 16.

One may also use the relation[18]

$$\langle k|z|p\rangle = -(1/\omega)\langle k|\nabla_z|p\rangle \tag{8}$$

to obtain

$$\sigma(\omega) = (8\pi/ck_0\omega)\,|\langle k|\nabla_z|p\rangle|^2 . \tag{9}$$

If states $|p\rangle$ and $|k\rangle$ are exact eigenstates of the total Hamiltonian, Eqs. (7) and (9) give $\sigma(\omega)$ exactly. The same diagrammatic expansion which is used to obtain $\langle k|z|p\rangle$, where $|p\rangle$ and $|k\rangle$ are again exact eigenstates, may also be used to obtain $\langle k|\nabla_z|p\rangle$. We may then write

$$\sigma(\omega) = (4\pi/c\omega)\,\mathrm{Im}\,\alpha'(\omega) , \tag{10}$$

where $\alpha'(\omega)$ is calculated like $\alpha(\omega)$ but with z replaced by ∇_z.

In calculating $\sigma(\omega)$ for the ground state of an atom using Eqs. (2) and (10), we note that only denominators with $+\omega$ contribute, since the denominators with $-\omega$ never vanish. The lowest-order contribution to $\sigma(\omega)$ comes from Eq. (9) and is given by the many-body diagram of Fig. 1(a). The heavy dot represents a matrix element of ∇_z or z according to whether we calculate $\alpha(\omega)$ or $\alpha'(\omega)$, and the horizontal line indicates the $-i\pi\delta$ contribution of Eq. (3). This notation has been used previously.[15,16,19] We note that every diagram contributing to $\sigma(\omega)$ has an odd number of horizontal lines. In the parts of the diagrams which contain no horizontal lines, denominators are treated by principal-value integration.

The diagrams which are first order in the correlation perturbation H_c' are shown in Figs. 1(b) and 1(c), where

$$H_c' = \sum_{i<j=1}^{N} r_{ij}^{-1} - \sum_{i=1}^{N} V(r_i) \tag{11}$$

and the single-particle potential $V(r_i)$ is chosen to account for the average interaction of the ith electron with the $N-1$ other electrons.[13] These diagrams also occur inverted and with exchange interactions. We also have diagrams like Fig. 1(a), but with insertions on either the hole line or the particle line.[14] Some diagrams which are second order in the H_c' perturbation are like those of Figs. 1(d)–1(h). We note that only Figs. 1(d) and 1(g) occur inverted; however, all may occur with exchange interactions. The effects of diagrams like Fig. 1(h) in which there are n interactions with H_c' and $n+1$ contributions from $-i\pi\delta$ (n even) may be summed exactly via a geometric series provided that the single-particle energy is the same for all hole lines.

When an electron is removed from the outer shell of a negative ion, the effect of the relaxation of the remaining outer-shell electrons may be significant.[6] Diagrams like those of Figs. 2(a) and 2(b) may account for this relaxation. Consider Fig. 2(a) where state $|p\rangle$ is the electron which is photoejected. If we let $|q\rangle$ be one of the remaining outer-shell electrons, then this diagram represents the effect on the wave function $|q\rangle$ owing to the removal of electron $|p\rangle$ and the presence of the continuum electron. Figures 2(a) and 2(b) may also contribute resonance effects.[16]

When the ground state of an atom (or ion) contains a partially filled subshell, resonances in the photoionization cross section occur owing to excitation of inner-shell electrons into vacancies in the partially filled shell. Resonances may also occur when ground-state electrons are excited into bound excited single-particle states.

The lowest-order diagram which gives a resonance contribution is that of Fig. 2(c) when state $|a\rangle$ is an inner-shell electron and state $|b\rangle$ is a vacant bound state. The bottom denominator is

$$D = \epsilon_a - \epsilon_b + \omega , \tag{12}$$

which vanishes at $\omega = \epsilon_b - \epsilon_a$. To incorporate the effects of the lifetime of the excited states, we note that the diagrams of Fig. 2(c), Fig. 2(d), and higher iterations form a geometric series with the ratio

$$-\frac{2i}{k}\,\frac{|\langle ak|v|bp\rangle|^2}{\epsilon_a - \epsilon_b + \omega} , \tag{13}$$

where we recognize the factor $(2/k)|\langle ak|v|bp\rangle|^2$ as the half-width of the resonance, $\frac{1}{2}\Gamma$.[20] This geo-

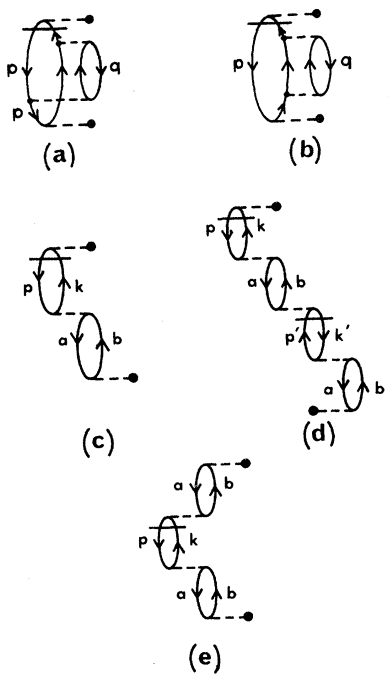

FIG. 2. (a) and (b) are two of the diagrams which alter the single-particle wave function $|q\rangle$ to account for the ejection of an electron in state $|p\rangle$; (c) is the lowest-order diagram which exhibits resonance behavior. The next iteration of diagram (c) is that shown in (d). This series may be summed geometrically to give back diagram (c) with a shifted denominator. Diagram (e) yields the largest contribution to the resonances. This diagram is also part of a series which may be summed to yield denominator shifts.

metric series then gives back Fig. 2(c) with the denominator of Eq. (12) shifted to give

$$D=\epsilon_a-\epsilon_b+\omega+\tfrac{1}{2}i\Gamma\ . \tag{14}$$

Similarly, such shifts occur in higher-order diagrams. The contribution to $\alpha(\omega)$ from Fig. 2(e) is

$$\frac{2i}{k}\frac{|\langle b|z|a\rangle|^2|\langle ak|v|bp\rangle|^2}{(\epsilon_a-\epsilon_b+\omega)^2}, \tag{15}$$

which when combined with higher-order diagrams of the same type gives

$$\frac{i\Gamma}{2}\frac{|\langle b|z|a\rangle|^2}{(\omega-\omega_0)^2+\frac{1}{4}\Gamma^2}, \tag{15a}$$

where ω_0 is the position of the resonance.

III. CALCULATIONS AND RESULTS

A. Single-Particle States and Ionization Energies

The single-particle states of O^- were calculated in the O^- ground-state configuration of $(1s)^2(2s)^2\times(2p)^5\,{}^2P$, where the vacancy in the $2p$ subshell has $m_l=-1$ and $m_s=-\frac{1}{2}$. All $l=0$ states were calculated using the Hartree–Fock (HF) equation for the $2s$ state. The result is the usual V^{N-1} potential[13] which gives a $1s$ single-particle energy lower than the true HF $1s$ energy, but a $1s$ wave function which differs only slightly from the HF wave function.[13] This difference in energy is easily understood, and corrections to this single-particle energy are made by including insertions on $1s$ hole lines.[13] We then obtain $\epsilon_{1s}=-20.1975$ a.u. as compared with Clementi's value of $\epsilon_{1s}=-20.1978$ a.u.[21] For ϵ_{2s} we obtain -0.8132 a.u. and $\epsilon_{2p}=-0.1288$ a.u.

The excited $l=1$ and 2 states were calculated by assuming the excitation of one of the ground-state $2p$ electrons and taking an average exchange interaction with the remaining $2p$ electrons. The V^{N-1} potential yielded no bound excited states. However, this does not imply that no bound excited states of O^- exist since in our calculation the potential is fixed and includes no rearrangement effects.

There are three well-defined thresholds in the photodetachment cross section of O^-, corresponding to the $(2p)^4\,{}^3P$, ${}^1D$, and ${}^1S$ multiplets of O, and we have used the experimental data for these ionization energies.[2] We expect that these experimental thresholds may be determined theoretically by inclusion of higher-order diagrams. We have taken the HF single-particle energies as the ionization energies for the $1s$ and $2s$ states.

B. Photodetachment Cross Section

The lowest-order contribution to $\sigma(\omega)$ is given by calculating the diagram shown in Fig. 1(a). The results, for both the length and velocity forms

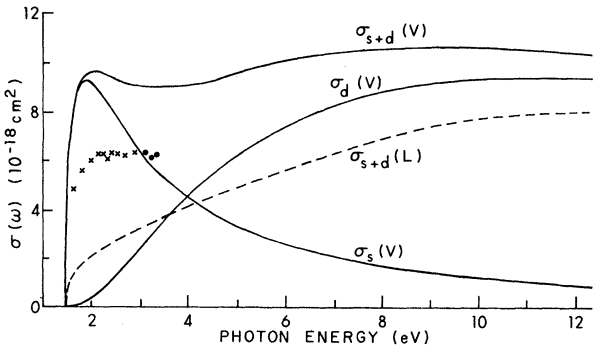

FIG. 3. Lowest-order cross sections which leave the oxygen atom in the ${}^3P$ state. Curves labeled (V) are calculated using the velocity form of the dipole matrix element. The curve labeled $\sigma_{s+d}(L)$ is the cross section using the length form. σ_s is the cross section for excitation into a continuum $l=0$ states, σ_d represents excitations into continuum $l=2$ states, and σ_{s+d} is the sum of both. Also given are the experimental results. The crosses are from Ref. 3 and the dots from Ref. 22.

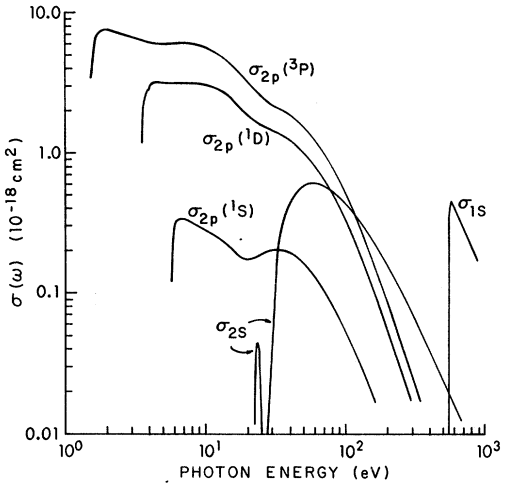

FIG. 4. Individual contributions to the photodetachment cross section from the $(1s)^2$, $(2s)^2$, and $(2p)^5$ subshells. The three $2p$ curves, designated by the multiplets of the residual oxygen atom, include all the diagrams of Fig. 1 except those effects which give rise to resonances.

of the dipole matrix element, for the residual ^3P multiplet of O from threshold to 12.5 eV, are shown in Fig. 3. These cross sections were obtained using Eqs. (1) and (10) and averaging over M_L. These results, when compared to the experimental cross section,[2,3,22] also shown in Fig. 3, indicate that the velocity form of the cross section may provide a better starting point, and thus place a smaller burden on the perturbation expansion. Therefore, we chose to complete the calculation using the velocity matrix element. In Fig. 3 we also present the separate contributions from excitations into $l=0$ and 2 states. In all other figures in this paper, a dashed line indicates the lowest-order $\sigma(\omega)$ using the velocity form.

In order to represent the three separate thresholds of the photodetachment cross section of O^- owing to the ejection of a $2p$ electron, we calculate the diagrams of Fig. 1 and project our results onto the three residual multiplets of O. We also include the normalization correction diagrams of Ref. 12, which are second order in the correlation perturbation H_c'. These normalization corrections were typically 6% reductions, and approached 10% for Figs. 1(b)–1(h) for the cases where all hole lines were $2p$ states. Figure 1(h) was calculated only for the case where the three hole lines were $2p$ states. Exchange diagrams and inverses were included where appropriate.

We have estimated the effects of the relaxation of the four remaining $2p$ orbitals following the ejection of a $2p$ electron by a consideration of the overlap integrals of the $2p$ orbitals before and after the interaction with the photon. For a single passive electron, $\langle 2p(O)|2p(O^-)\rangle = 0.9874$, which when squared and then raised to the fourth power gave an over-all factor of 0.9038 for all diagrams in which a $2p$ electron was photoejected. In this manner we have approximated the effects of diagrams like those of Figs. 2(a) and 2(b) and other higher-order diagrams which alter the wave functions of the passive $2p$ electrons. No attempts were made to account for relaxation when either a $1s$ or $2s$ electron was photoejected.

The final cross sections for each of the subshells of O^- are given in Fig. 4, where no resonance effects have been included. Resonance effects are contributed by diagrams like Figs. 2(c)–2(e) when state $|a\rangle$ is an inner-shell electron, and state $|b\rangle$ is a bound state vacant in the ground state of O^-. The three $2p$ cross sections include all the correlation effects of Figs. 1(b)–1(h), while the $1s$ and $2s$ cross sections include only Fig. 1(a), since it was expected that correlations of the inner-shell electrons would not affect these particular cross sections to a great extent. The $2s$ cross section has two maxima with a zero in between, since the $\langle kp|\nabla_z|2s\rangle$ matrix element changes sign at $k \simeq 0.5a_0^{-1}$

TABLE I. Effects of correlations on the photodetachment cross section $O^- + \omega \rightarrow O(^3P) + e$. Resonance effects of Figs. 2(c)–2(e) not included in this table.

Photon energy (eV)	σ [Fig. 1(a)] (10^{-18} cm^2)	σ [Figs. 1(a)–1(c)] (10^{-18} cm^2)	σ [Figs. 1(a)–1(g)] (10^{-18} cm^2)[a]	σ [Figs. 1(a)–1(h)] (10^{-18} cm^2)[a]
1.498	4.319	3.291	3.405	3.405
1.770	9.188	6.933	7.251	7.251
2.008	9.644	7.122	7.545	7.545
3.641	9.079	4.464	6.325	6.354
10.171	10.667	2.764	5.991	5.605
21.055	8.131	3.412	3.425	3.037
36.293	4.508	3.319	2.207	2.020
55.884	2.172	2.008	1.443	1.366
123.909	0.346	0.382	0.321	0.314
341.589	0.018	0.020	0.017	0.017

[a]Normalization effects of Ref. 12 and relaxation effects of Figs. 2(a) and 2(b) also included.

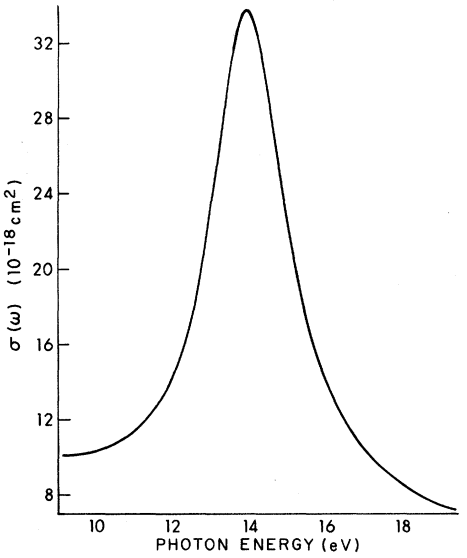

FIG. 5. Final cross section in the region of the $2s \rightarrow 2p$ resonance.

($\omega \simeq 26$ eV).

The diagrams of Figs. 1(b) and 1(c), which are first order in the correlation perturbation H_c', have the largest effect on the lowest-order cross section. In general, these diagrams subtract from our lowest-order cross section out to about 67 eV, after which they become additive. The effects of correlations on the ^3P cross section are shown in Table I. Similar effects were found for the ^1D and ^1S cross sections.

The resonance contributions of Figs. 2(c) and 2(e) with shifted denominators as in Eqs. (14) and (15a) were also included in this calculation. The position and width of a given resonance may be determined from the techniques leading to Eqs. (12)–(15). The position and width may also be determined by considering the energy differences before and after the resonance transition.[20] After either a $1s \rightarrow 2p$ or $2s \rightarrow 2p$ transition, the negative ion is in a ^2S atomic state. The correlation energy of the ^2S state has both a real and an imaginary part, where the real part contributes to the resonance position ω_0 and the imaginary part is proportional to the linewidth $\Gamma(\omega_0)$.[20] In lowest order,

$$\Gamma_0 = \Gamma(\omega_0) = (4/k_0)\,|\langle ak_0|v|qp\rangle|^2, \tag{16}$$

where

$$k_0 = [2(\epsilon_p + \epsilon_q - \epsilon_a)]^{1/2}, \tag{17}$$

$|a\rangle$ is the now vacant inner-shell state, $|p\rangle$ is the electron which is ejected, and $|q\rangle$ is any other occupied state. We note that for Eqs. (16) and (17) to have meaning, the photon energy ω must be greater than $\epsilon_p + \epsilon_q - \epsilon_a$. Equation (16) is the lowest-order result; higher-order terms should also be included. This approach is identical to our previous development in terms of the polarizability diagrams of Figs. 2(c)–2(e).

For the $2s \rightarrow 2p$ resonance, we have calculated $\omega_0 = 0.5178$ a.u., or 14.089 eV. For the linewidth at ω_0, the lowest-order term calculated using Eq. (13) gave 0.1330 a.u., and for our final result $\Gamma_0 = 0.0899$ a.u., or 2.45 eV. The total cross section $\sigma(\omega)$ in the neighborhood of the $2s \rightarrow 2p$ resonance is shown in Fig. 5 and includes the contributions of Figs. 2(c)–2(e). Near ω_0, Fig. 2(c) was on the order of 0.1×10^{-18} cm^2, compared to an over-all magnitude of 33.7×10^{-18} cm^2, which is primarily due to the contribution from the diagram of Fig. 2(e). The peak of the $2s \rightarrow 2p$ resonance occurs at 13.932 eV, which is slightly lower than the ω_0 of 14.089 eV. This is caused by the very rapid falloff of terms already included which have no resonance contributions. This also explains the lower magnitude on the high-energy side of the resonance.

The position and width of the resonance caused by the degeneracy of the $1s \rightarrow 2p$ and $2p \rightarrow ks$ or kd transitions were also calculated and gave $\omega_0 = 546.105$ eV, and $\Gamma_0 = 0.037$ eV.

Our final cross section, including the normalization corrections,[12] from threshold to 1.1 keV is shown as the solid curve in Fig. 6. Also presented is our lowest-order result [the diagram of Fig. 1(a) only]. At approximately 200 eV, the total cross section becomes virtually indistinguishable from the lowest-order result, except in the region of the $1s \rightarrow 2p$ resonance. A comparison of our lowest-order and total cross sections is presented in Table II.

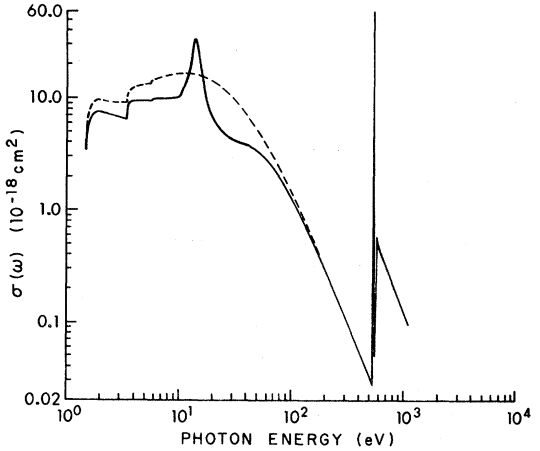

FIG. 6. Cross sections from threshold to 1.1 keV. The solid curve represents our final result, and the dashed curve is our lowest-order result.

TABLE II. Comparison of lowest-order and final results for the photodetachment cross section of O^-.

Photon energy (eV)	Lowest-order $\sigma(\omega)$ (10^{-18} cm^2)	Final $\sigma(\omega)$ (10^{-18} cm^2)
1.465[a]	0.000	0.000
1.498	4.319	3.405
1.600	7.520	5.940
1.676	8.538	6.745
2.008	9.644	7.546
2.688	9.200	6.876
3.431[b]	9.064	6.453
3.465	10.309	7.606
3.848	12.239	9.283
4.655	12.966	9.471
5.660[c]	13.752	9.439
5.796	14.096	9.678
6.204	14.548	9.813
9.061	16.357	10.065
12.326	16.760	16.213
13.605	16.571	31.600
13.932	16.501	33.720
14.089[d]	16.465	33.401
15.782	15.979	15.386
17.958	15.174	8.606
20.081	14.278	6.618
22.312[e]	13.304	5.598
23.945	12.606	5.150
32.326	9.371	4.142
60.080	3.922	2.809
128.105	0.872	0.821
293.541	0.127	0.124
541.479	0.027	0.036
545.561	0.026	0.773
546.105[f]	0.026	161.020
546.241	0.026	11.378
546.649	0.026	0.779
549.642[g]	0.031	0.048
552.363	0.347	0.351
571.410	0.489	0.489
876.380	0.177	0.177
1107.665	0.096	0.096

[a] ^3P threshold.
[b] ^1D threshold.
[c] ^1S threshold.
[d] Location of $2s \rightarrow 2p$ resonance.
[e] Location of $2s$ edge.
[f] Location of $1s \rightarrow 2p$ resonance.
[g] Location of $1s$ edge.

In Fig. 7 we present the photodetachment cross section of O^- from threshold to 12.5 eV in order to provide detailed results in the region of the three $2p$ excitation thresholds. Also presented are the experimental results,[2,3,22] and the calculation of Henry.[8] We find very good agreement in the reproduction of the ^1D threshold; however, our results are some 25% too large at the peak of the ^3P threshold. One possibility for this result is our approximation of diagrams of the type shown in Figs. 2(a) and 2(b), and our omission of other diagrams.[16] It should also be noted that the experimental results may contain normalization errors of up to 10%.[3]

IV. DISCUSSION

This paper represents the first calculation of the photodetachment cross section of O^- which includes a many-body treatment of correlation effects. This treatment of correlation effects introduces resonances in a natural manner. As in the calculation of Henry,[8] we found that in lowest order the length form of the dipole matrix element yielded results which were significantly lower than experiment. We therefore chose the velocity form of the dipole matrix element as a better starting point for the calculation.

Henry's calculation,[8] which used the polarized orbital method of Temkin,[7] gave good results in the ^3P threshold region for the velocity form, but not for the length form. Garrett and Jackson[6] used first-order perturbation theory to obtain a polarization potential from the perturbation of the bound-state system by the detached electron. They then adjusted the coefficients of the exchange terms in the HF equation to obtain a $2p$ single-particle wave function which had an energy equal to the ionization energy of O^- (1.465 eV). This calculation, using the length form of the dipole matrix element, also gave good results in the region near the ^3P threshold.

The calculations discussed above, however, did not predict the resonances which arise from the excitation of inner-shell electrons to the $2p$ state vacant in the ground state of O^-. Although our potential yields no bound excited single-particle states, this does not preclude the existence of other resonances in the photodetachment cross section of O^-. Our method yields only two reso-

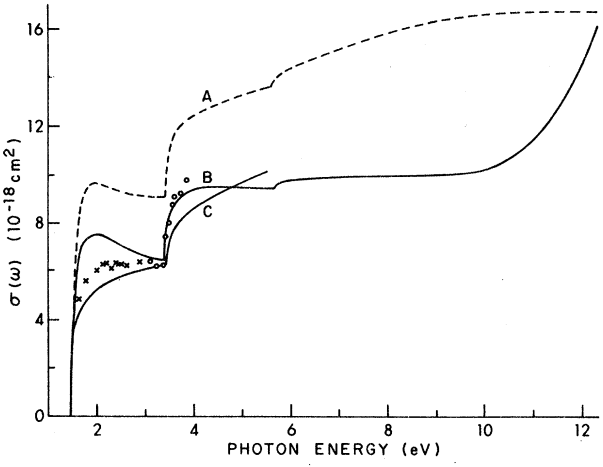

FIG. 7. Detailed presentation of cross sections from threshold to 12.5 eV. The dashed curve A is our lowest-order result, the solid curve B is our final cross section, and C is the result of Ref. 8 for comparison. The crosses and dots are the experimental results of Refs. 3 and 22, respectively.

nances, one caused by the degeneracy of the $1s \rightarrow 2p$ and $2p \rightarrow ks$ or kd transitions, and the other caused by the degeneracy of the $2s \rightarrow 2p$ and $2p \rightarrow ks$ or kd transitions. Although we predict the $2s \rightarrow 2p$ resonance to lie at 14.089 eV, and the $1s \rightarrow 2p$ resonance to lie at 546.105 eV, there may be errors owing to the lack of higher-order terms which shift the positions of these resonances.[14] This lack of higher-order terms may also introduce errors in our values of $\Gamma_0 = 2.45$ and 0.037 eV for the $2s \rightarrow 2p$ and $1s \rightarrow 2p$ resonances, respectively. We expect, however, that these two resonances do exist, and it is hoped that experimental work on the photodetachment of O^- will eventually give an accurate determination of the positions and widths of these and any other resonances.

ACKNOWLEDGMENTS

We would like to thank Dr. J. H. Miller for several helpful discussions and also to thank him and Dr. G. J. Klem for assistance with the angular momentum computer programs. In addition, we would also like to thank Dr. T. E. H. Walker, Dr. A. Ron, Dr. J. J. Chang, and Dr. M. Siegel for helpful discussions.

---

†Research supported by the Aerospace Research Laboratories, Office of Aerospace Research, U. S. Air Force Contract No. F33615-69-C-1048.

*Present address: Piedmont Virginia Community College, Box 5183, Charlottesville, Va. 22903.

[1]D. R. Bates and H. S. W. Massey, Phil. Trans. Roy. Soc. London A239, 269 (1943).

[2]L. M. Branscomb, D. S. Burch, S. J. Smith, and S. Geltman, Phys. Rev. 111, 504 (1958).

[3]S. J. Smith, in *Proceedings of the Fourth International Conference on Ionization Phenomena in Gases, Uppsala, Sweden* (North-Holland, Amsterdam, 1960), p. 219.

[4]J. W. Cooper and J. B. Martin, Phys. Rev. 126, 1482 (1962).

[5]E. J. Robinson and S. Geltman, Phys. Rev. 153, 4 (1967).

[6]W. R. Garrett and H. T. Jackson, Jr., Phys. Rev. 153, 28 (1967).

[7]A. Temkin, Phys. Rev. 107, 1004 (1957).

[8]R. J. W. Henry, Phys. Rev. 162, 56 (1967).

[9]K. A. Brueckner, Phys. Rev. 97, 1353 (1955).

[10]J. Goldstone, Proc. Roy. Soc. (London) A239, 267 (1957).

[11]H. P. Kelly, Phys. Rev. 131, 684 (1963).

[12]H. P. Kelly, Phys. Rev. 136, B896 (1964).

[13]H. P. Kelly, Phys. Rev. 144, 39 (1966).

[14]H. P. Kelly, Phys. Rev. 182, 84 (1969).

[15]H. P. Kelly and A. Ron, Phys. Rev. Letters 26, 1359 (1971).

[16]H. P. Kelly and A. Ron, Phys. Rev. A 5, 168 (1972).

[17]U. Fano and J. W. Cooper, Rev. Mod. Phys. 40, 441 (1968).

[18]H. A. Bethe, *Intermediate Quantum Mechanics* (Benjamin, New York, 1964), p. 148.

[19]G. Wendin, J. Phys. B 3, 455 (1970); 3, 466 (1970).

[20]R. L. Chase, H. P. Kelly, and H. S. Köhler, Phys. Rev. A 3, 1550 (1971).

[21]E. Clementi and A. D. McLean, Phys. Rev. 133, A419 (1964).

[22]L. M. Branscomb, S. J. Smith, and G. Tisone, J. Chem. Phys. 43, 2906 (1963).